SUPPORTING INFORMATION

for

Evolution of Magnetic Particulate Matter during its Emission Process in Thermal Power Plants

Hang Yang[1,3], Qinghua Zhang[1], Jiayuan Wu[2], Lin Liu[1,3], Dingyi Wang[1], Dawei Lu[1,3], Weichao Wang[1,3], Ke Min[1], Weichan Zhang[1,3], Qian Liu[1,3,4]*, Yi Yang[2]*, Guibin Jiang[1,3]

[1] *State Key Laboratory of Environmental Chemistry and Ecotoxicology, Research Center for Eco-Environmental Sciences, Chinese Academy of Sciences, Beijing 100085, China*

[2] *Key Laboratory of Geographic Information Science (Ministry of Education), School of Geographic Sciences, East China Normal University, Shanghai 200241, China;*

[3] *College of Resources and Environment, University of Chinese Academy of Sciences, Beijing 100049, China*

[4] *Institute of Environment and Health, Jianghan University, Wuhan 430056, China*

Email: qianliu@rcees.ac.cn (Q. Liu); yyang@geo.ecnu.edu.cn (Y. Yang)

Contents

1. **Supplementary Experimental Section**
2. **Supplementary Tables S1-S4**
3. **Supplementary Figures S1-S11**

1. Supplementary Experimental Section

Estimation of potential experimental errors caused by the CME system

Considering that small magnetic particles embedded in large non-magnetic particles (e.g., aluminosilicate) may escape from the magnetic extraction, we designed an experiment to assess the underestimate of magnetic content caused by this part of particles. Briefly, after the first round of extraction, the non-magnetic residues of FA were transferred to 40 mL of KOH solution and digested at 90 °C for 12 h. The mixture was treated by the CME again, and the embedded MPs could be released and their content was quantified by ICP-MS. In this way, this part of experimental errors was estimated to be 3.5 ± 0.8% (n = 5).

We have also assessed the overestimate of magnetic content due to the possible presence of iron in other phases after acetic acid purification. Briefly, 10 mg of magnetic extracts were dispersed in 10 mL of KOH and heated at 90 °C for 12 h to maximize the dissolution of iron presented in the other phases (e.g., aluminosilicate). The purified magnetic extracts in the KOH solution were extracted by the CME system again and the iron dissolved in KOH and magnetic extracts was quantified by ICP-MS. In this way, this part of experimental error was estimated to be 3.3 ± 1.7% (n = 3).

2. Supporting tables

Table S1. Information about the fuels fed in three units.

Units from Power plants	Fuel	Proximate analysis (%)				Iron concentration (μg/g)	iron-bearing mineral compositions (XRD)				
		M_{ad}	A_{ad}	V_{ad}	FC_{ad}		Pyrite	Siderite	Ankerite	Magnetite	Himatite
PP1.1	Shanxi coal	7.80	20.2	24.9	47.1	1.50×10^3	√	√	√	√	×
PP1.2	Indonesian coal	7.13	21.6	27.4	43.8	6.75×10^3	√	√	√	√	√
PP2	Oil shale	10.5	69.8	17.5	2.25	2.63×10^5	√	√	√	√	×

Note: M_{ad}: moisture;

A_{ad}: ash;

V_{ad}: volatile matter;

FC_{ad}: fixed carbon;

Subscript ($_{ad}$) represents air dry basis;

√: iron-bearing mineral compositions detected by XRD;

×: iron-bearing mineral compositions undetected by XRD.

Table S2. Iron percentages (%) of magnetic particles (Fe_2O_3 and γ-Fe_2O_3) to total iron-bearing species in FA collected from the graded ash hoppers.

PP1.1			PP1.2			PP2		
Collector	**Fe_3O_4**	**γ-Fe_2O_3**	**Collector**	**Fe_3O_4**	**γ-Fe_2O_3**	**Collector**	**Fe_3O_4**	**γ-Fe_2O_3**
ESP **I**	48.7%	2.91%	ESP **I**	46.9%	2.52%	ESP **I**	46.9%	10.6%
ESP **II**	40.0%	2.52%	ESP **II**	47.5%	3.07%	ESP **II**	56.2%	7.72%
ESP **III**	36.7%	1.82%	ESP **III**	31.8%	1.57%	BF **I**	37.1%	9.88%
ESP **IV**	40.7%	1.77%	ESP **IV**	44.1%	2.28%	BF **II**	41.9%	8.91%
ESP **V**	52.8%	3.74%	ESP **V**	65.9%	4.52%			

Abbreviations: ESP: Electrostatic precipitator; BF: bag filter.

Table S3. The number percentage of PM_1 contribution to the magnetic extracts (PM_1/magnetic extracts) from PP-derived FAs. Particle size statistics based on SEM images with ~1000 particles, and measured in triplicate (n = 3).

PP1.1		PP1.2		PP2	
Sample	**PM_1/magnetic extracts (mean ± SD, n =3)**	**Sample**	**PM_1/magnetic extracts (mean ± SD, n =3)**	**Sample**	**PM_1/magnetic extracts (mean ± SD, n =3)**
FA I	21.4 ± 5.7	**FA I**	17.5 ± 3.5	**FA I**	12.3 ± 4.4
FA II	17.3± 8.8	**FA II**	25.6 ± 5.4	**FA II**	28.9 ± 6.6
FA III	9.98 ± 9.2	**FA III**	25.6 ± 6.6	**FA III**	19.2 ± 7.3
FA IV	22.0 ± 1.9	**FA IV**	26.0 ± 3.1	**FA IV**	33.9 ± 5.1
FA V	31.9 ± 3.2	**FA V**	31.7 ± 1.8		

Table S4. Concentrations of extracted Fe_3O_4 in graded FAs and their associated elements.

Boiler system	Sample	Concentration									
		(μg/g)						(ng/g)			
		Fe	Al	Ti	Mn	Ba	Zn	Cr	V	Ni	Co
PP1.1	FA I	1.85×10^4	1.43×10^4	5.12×10^2	30.6	34.0	23.1	6.75×10^3	5.31×10^3	1.33×10^3	6.40×10^2
	FA II	1.00×10^4	8.00×10^3	3.93×10^2	21.6	14.9	42.3	3.84×10^3	5.05×10^3	9.82×10^2	-
	FA III	9.30×10^4	6.29×10^3	3.59×10^2	19.7	11.0	14.5	3.14×10^3	4.03×10^3	1.14×10^3	-
	FA IV	1.02×10^4	8.83×10^3	4.74×10^2	22.3	24.6	13.7	5.29×10^3	5.77×10^3	2.88×10^2	-
	FA V	3.90×10^4	1.83×10^4	1.11×10^3	3.77×10^2	1.00×10^2	63.8	1.79×10^4	1.69×10^4	1.04×10^4	5.59×10^3
PP1.2	FA I	1.37×10^4	1.28×10^4	6.90×10^2	45.5	27.1	21.5	4.49×10^3	8.33×10^3	2.50×10^3	1.19×10^3
	FA II	2.45×10^4	1.54×10^4	9.66×10^2	2.57×10^2	74	34.2	1.42×10^4	1.68×10^4	8.53×10^3	5.13×10^3
	FA III	9.20×10^3	7.12×10^3	3.87×10^2	19.6	13.7	27.6	3.86×10^3	4.65×10^3	1.85×10^2	-
	FA IV	2.72×10^4	1.55×10^4	9.85×10^2	1.28×10^2	87.4	35.7	1.91×10^4	1.99×10^4	8.28×10^3	6.45×10^3
	FA V	4.24×10^4	1.73×10^4	1.16×10^3	3.94×10^2	1.03×10^2	38.3	2.01×10^4	1.92×10^4	1.21×10^4	6.32×10^3
PP2	FA I	2.83×10^4	1.97×10^4	2.33×10^3	7.13×10^2	3.20×10^2	63.2	4.69×10^4	4.14×10^4	3.63×10^4	1.26×10^4
	FA II	3.11×10^4	1.36×10^4	1.94×10^3	7.83×10^2	1.74×10^2	58.9	1.51×10^4	3.06×10^4	4.21×10^4	1.06×10^4
	FA III	2.11×10^4	1.22×10^4	1.35×10^3	5.66×10^2	2.31×10^2	41.4	2.93×10^4	2.43×10^4	2.18×10^4	7.68×10^3
	FA IV	2.38×10^4	9.53×10^3	1.23×10^3	5.62×10^2	1.24×10^2	41.0	2.70×10^2	2.06×10^4	2.35×10^4	8.05×10^3

Note: "-" indicates that the value was below quantification limits.

3. Supporting figures

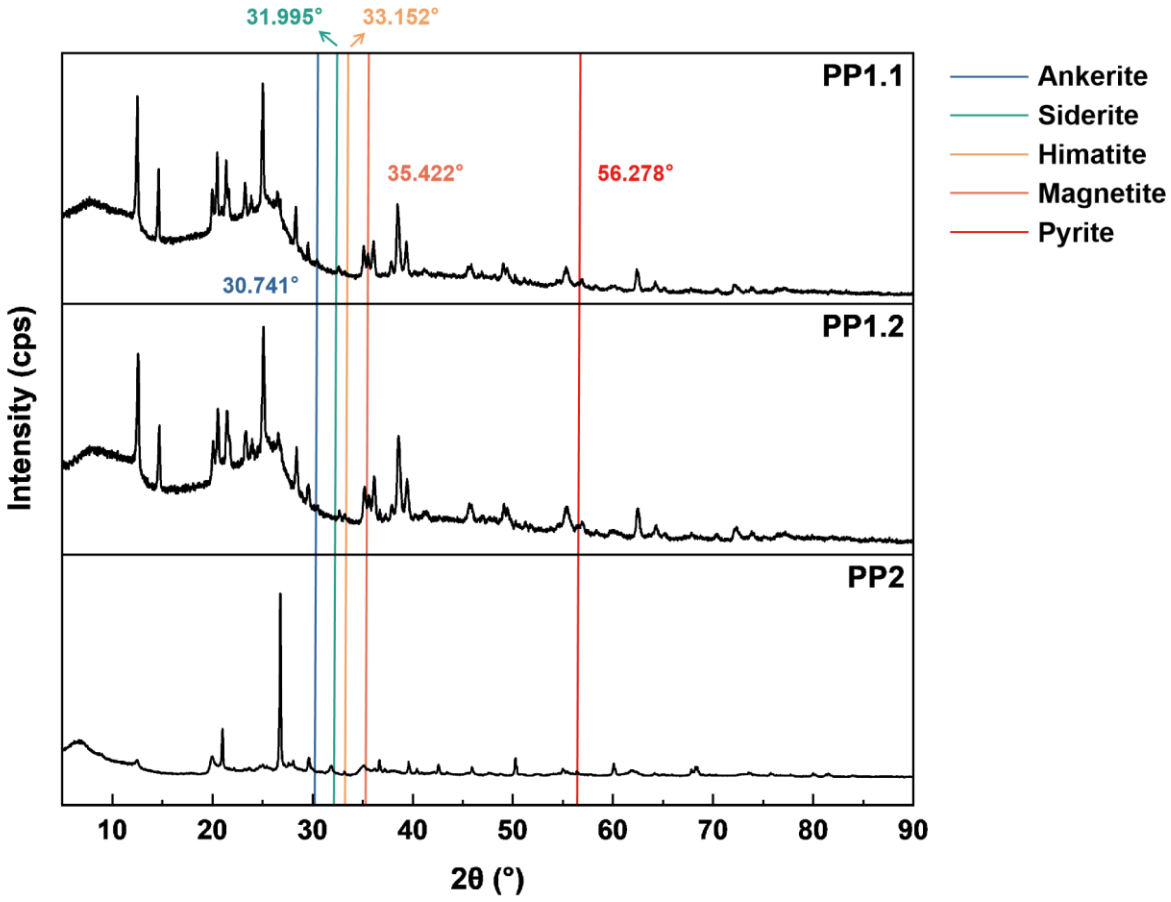

Figure S1. XRD patterns of fuels used by the three boilers. The characteristic peaks of major iron-bearing minerals are labelled with different colored lines. The detection results of iron bearing mineral compositions are shown in Table S1.

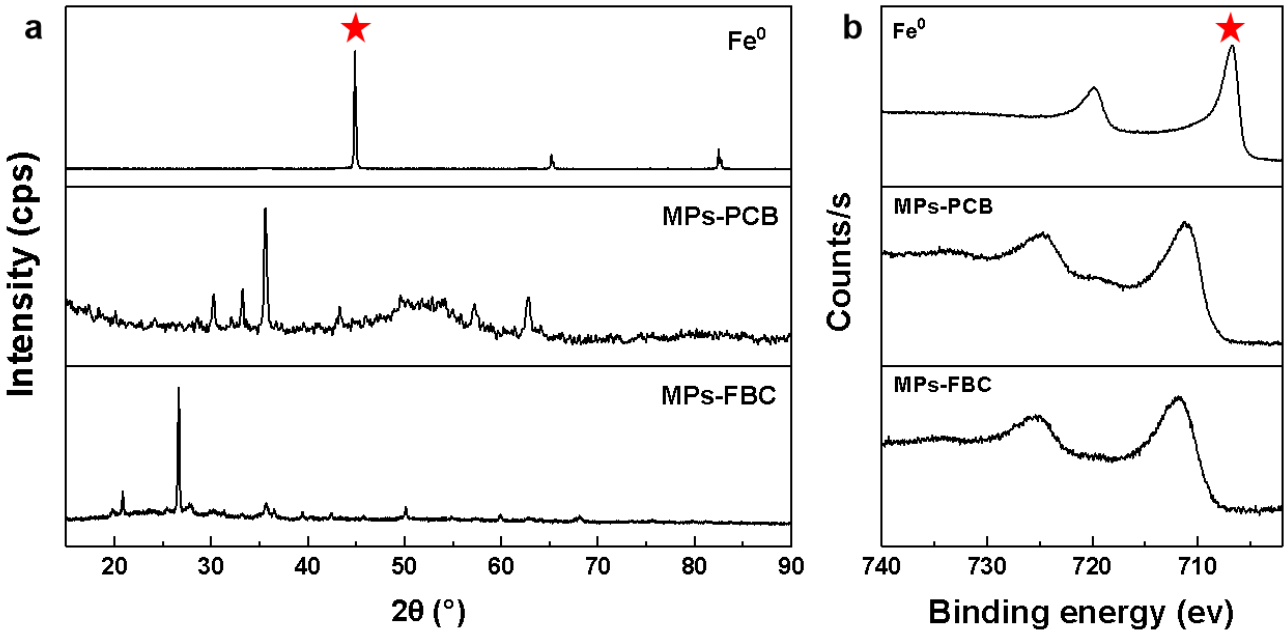

Figure S2. Identification of magnetic extracts from the PP-derived FA. (a) XRD patterns of Fe^0 and the magnetic extracts. (b) XPS spectra of Fe^0 and the magnetic extracts. The characteristic peaks of Fe^0 are labelled with stars. Results indicated that the magnetic extracts from power plant-derived FA did not contain Fe^0. PCB: pulverized coal boiler; FBC: fluidized bed combustor.

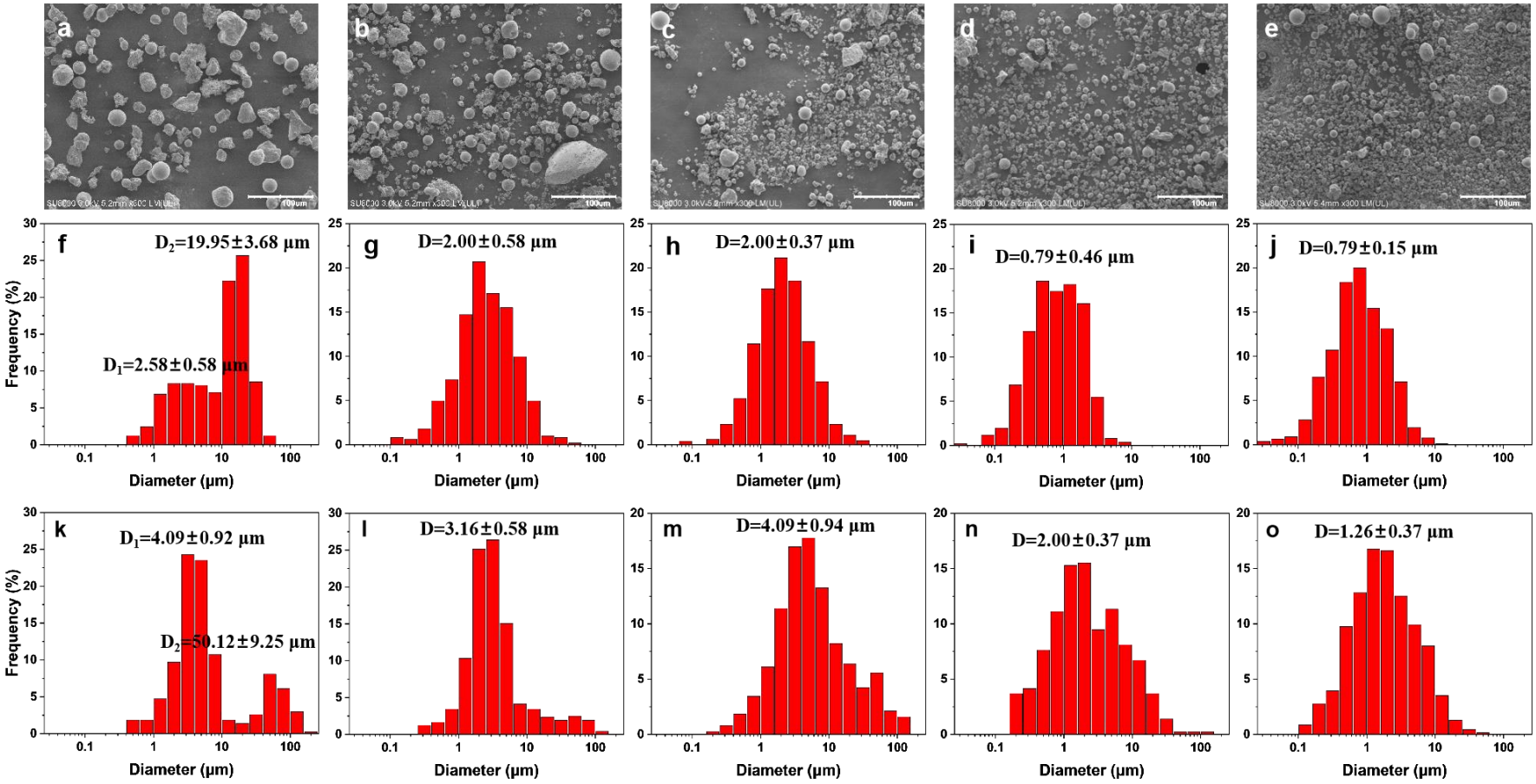

Figure S3. Particle size distribution of graded FA samples and corresponding magnetic extracts collected from PCB. (a-e) Typical SEM images of FA I-FA V. (f-j) Particle size distribution of graded FA samples. (k-o) Particle size distribution of MPs in graded FA samples. The particle size distribution statistics were counted based on SEM images with ~1000 particles. FA I - V: graded fly ash samples collected from sequential hoppers.

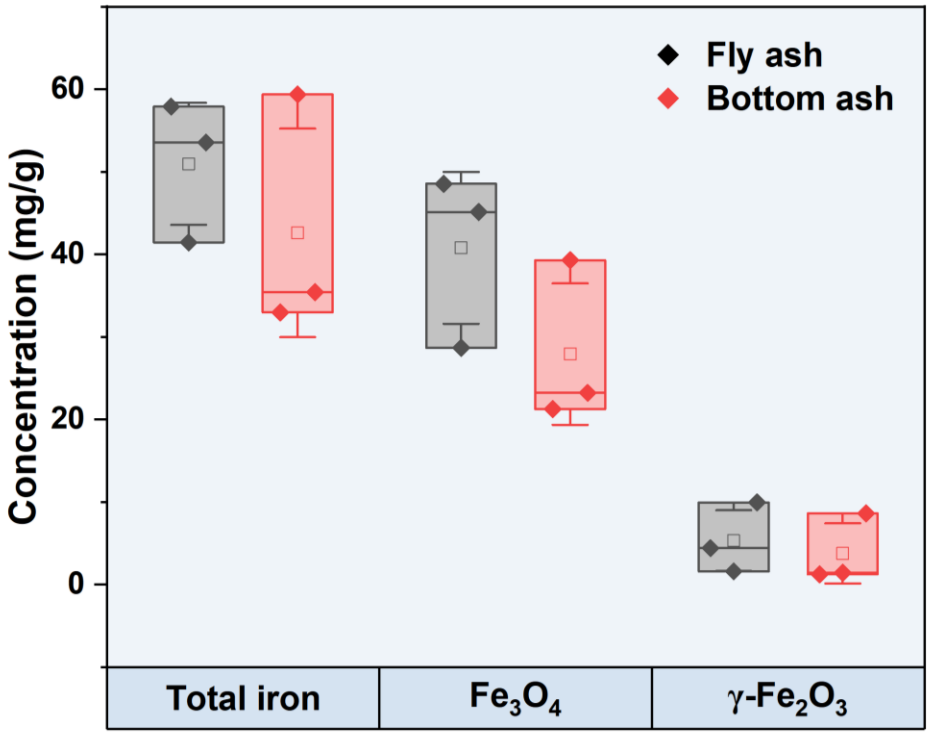

Figure S4. Average concentrations of iron-bearing substances (total iron, Fe_3O_4, and γ-Fe_2O_3) in bottom ash (BA) and the intercepted FA samples collected from PP1 and PP2. The average concentration of intercepted FA was calculated referring to Eq. (2). The intercepted FA means the total FAs collected by dust removal systems.

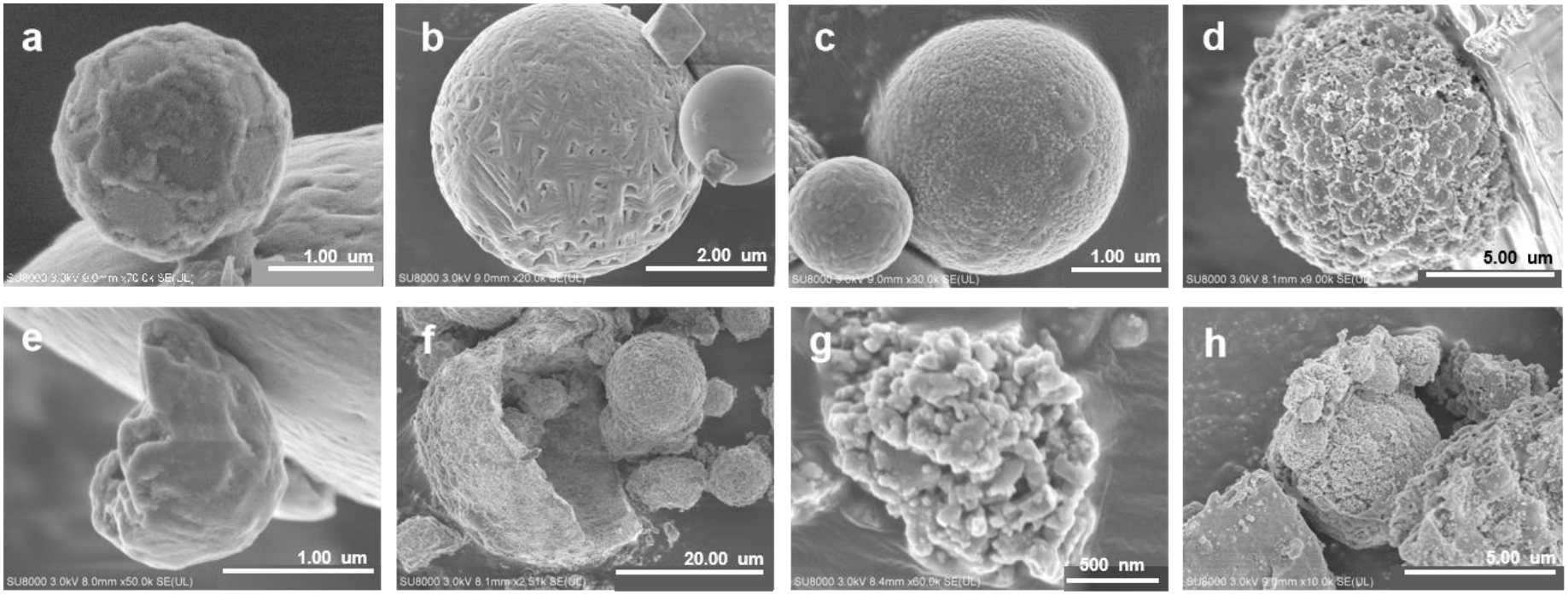

Figure S5. Typical morphology of PP-derived magnetic particles. (a) Particles with polygonal surfaces, (b) particles with striated surfaces, (c) particles with fine-grained surfaces, (d) cluster of particles with a grape-like morphology, (e) irregular particles, and (f) broken hollow-shell particles from PP1 with PCB. (g) Irregular particles and (h) nearly spherical particles from PP2 with FBC.

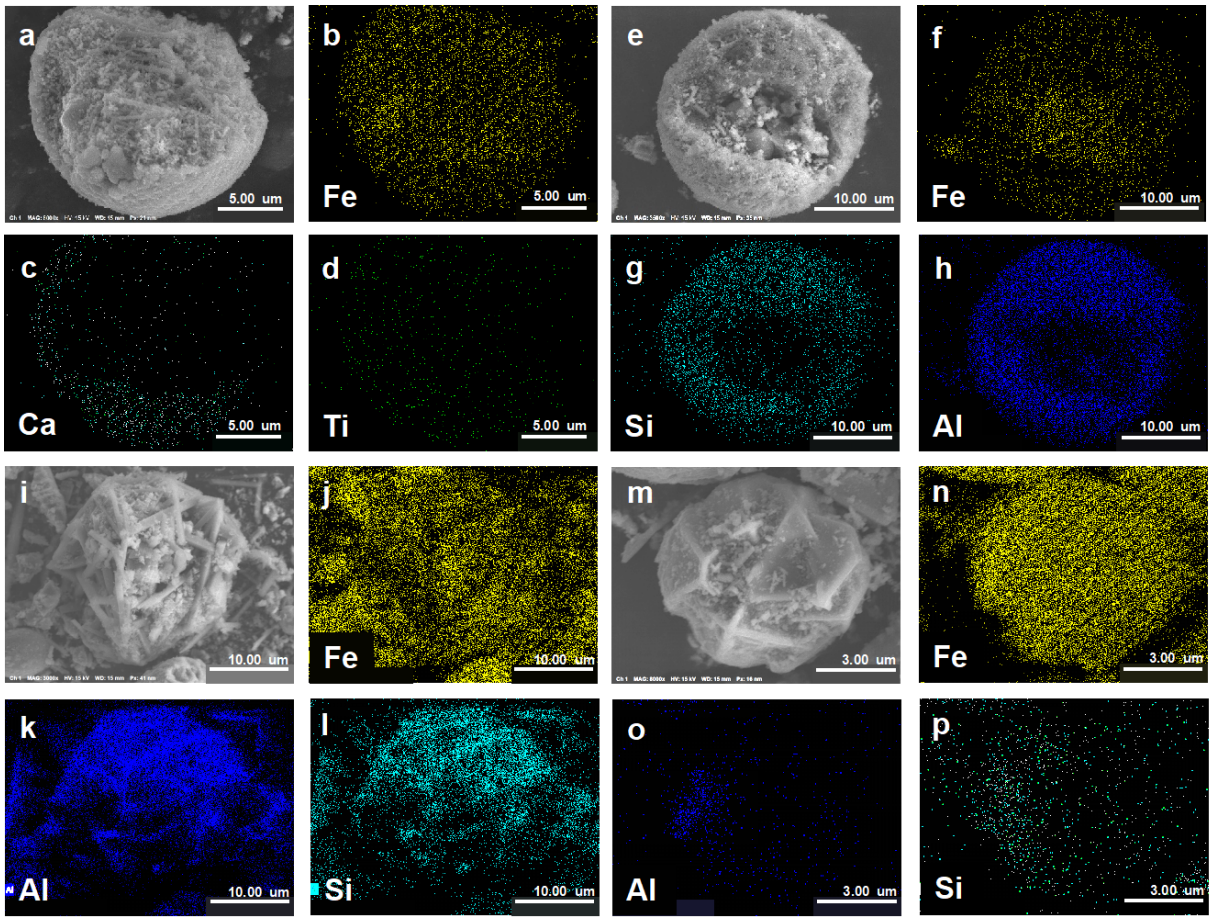

Figure S6. Elemental mapping of imperfect magnetic particles with different structures. (a-d) Agglomerated particle with rod-shaped sub-particles and nanosized sub-particles, and a spherical particles-formed shell, (e-h) particle with agglomerated shell and hollow structure, (i-l) particle agglomerated by rod-shaped sub-particles, and (m-p) particle agglomerated by cubelike sub-particles derived from PCB and the corresponding EDX-mapping. From the exposed internal structure of the imperfect particles, it is clear that the large particles formed via the agglomeration of sub-particles.

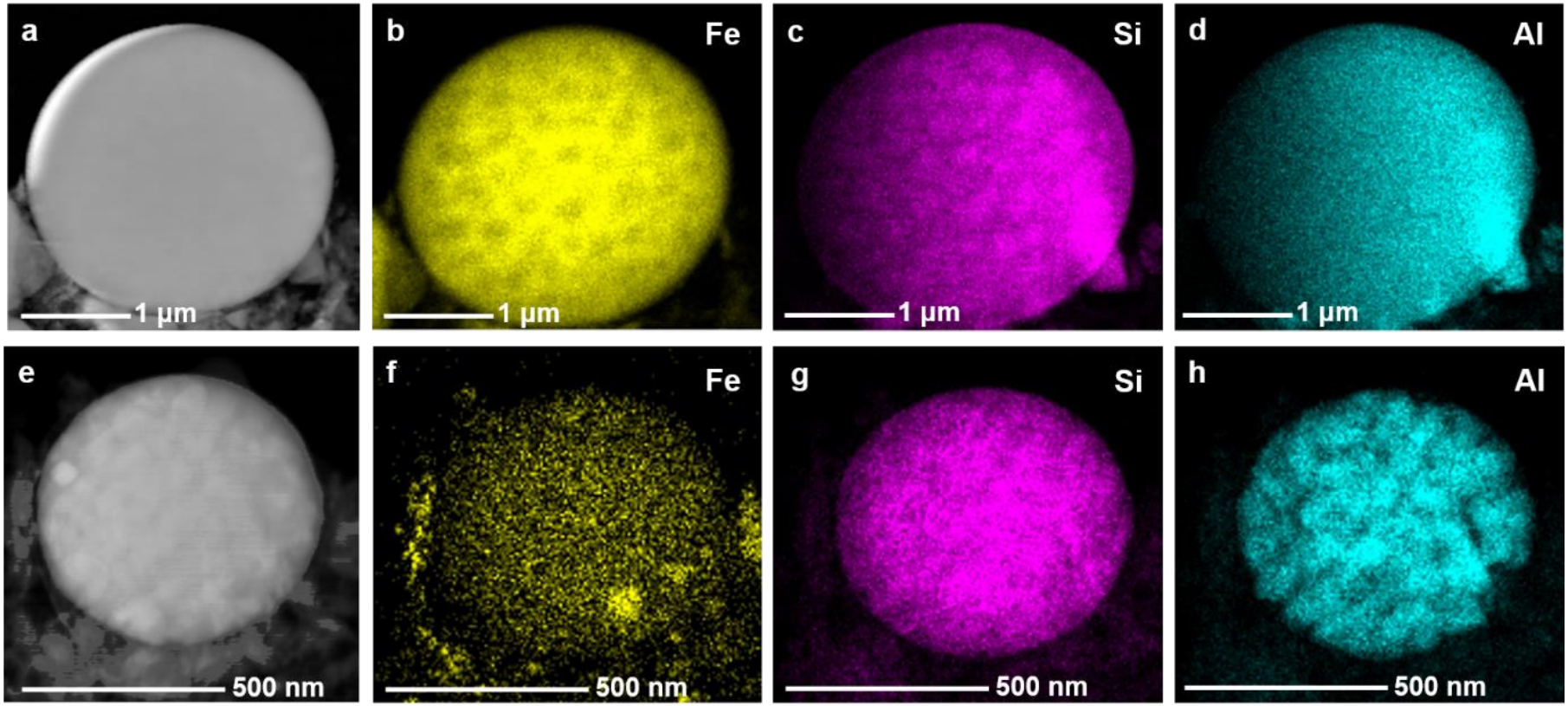

Figure S7. Characterization of microstructures of PP-derived magnetic particles with nanosized sub-particles. HAADF-STEM image and EDXS mapping of magnetic agglomerates (aluminosilicate particles in Fe_3O_4 matrix) from (a-d) PP1 with PCB and (e-h) from PP2 with FBC.

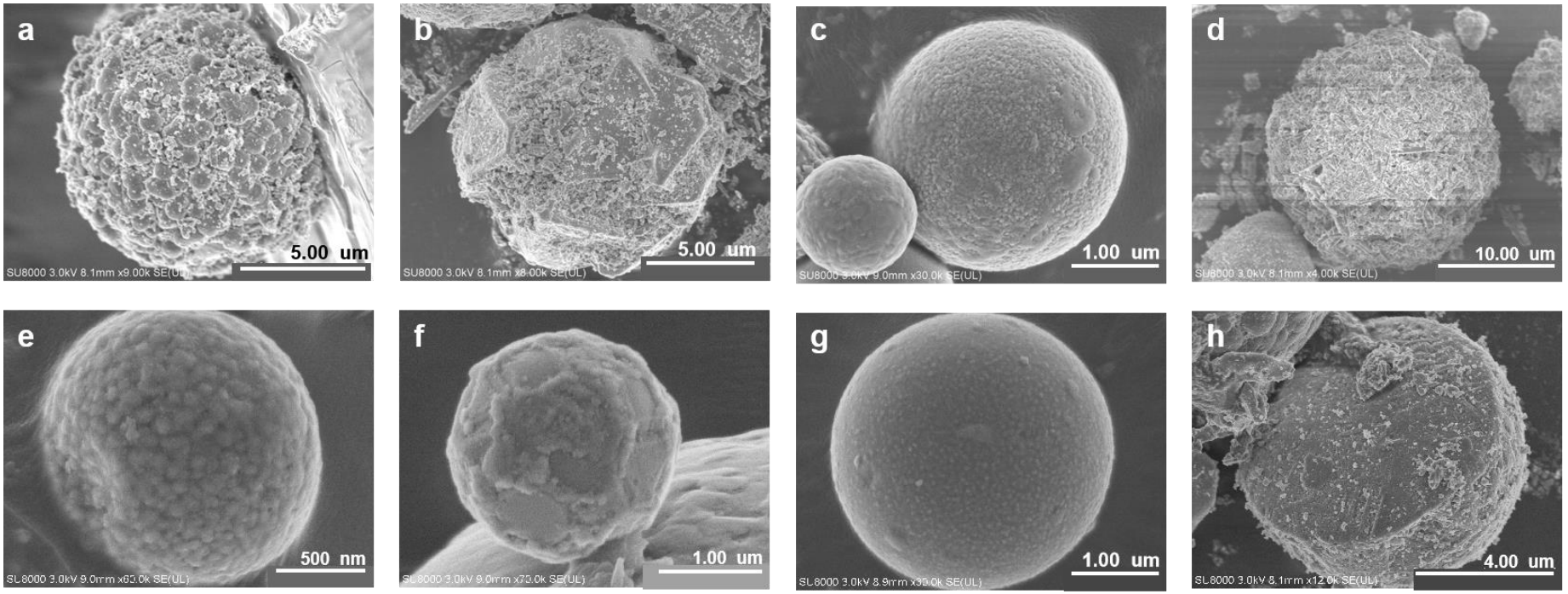

Figure S8. Typical morphologies of loose magnetic particles and their corresponding fused particles in different states from pulverized coal boiler. (a-d) Initial loose particles. (e-h) The corresponding fused particles after coagulation with similar but more compact microstructures. Such an observation gives valuable information about the morphology evolution of MPs during the combustion process.

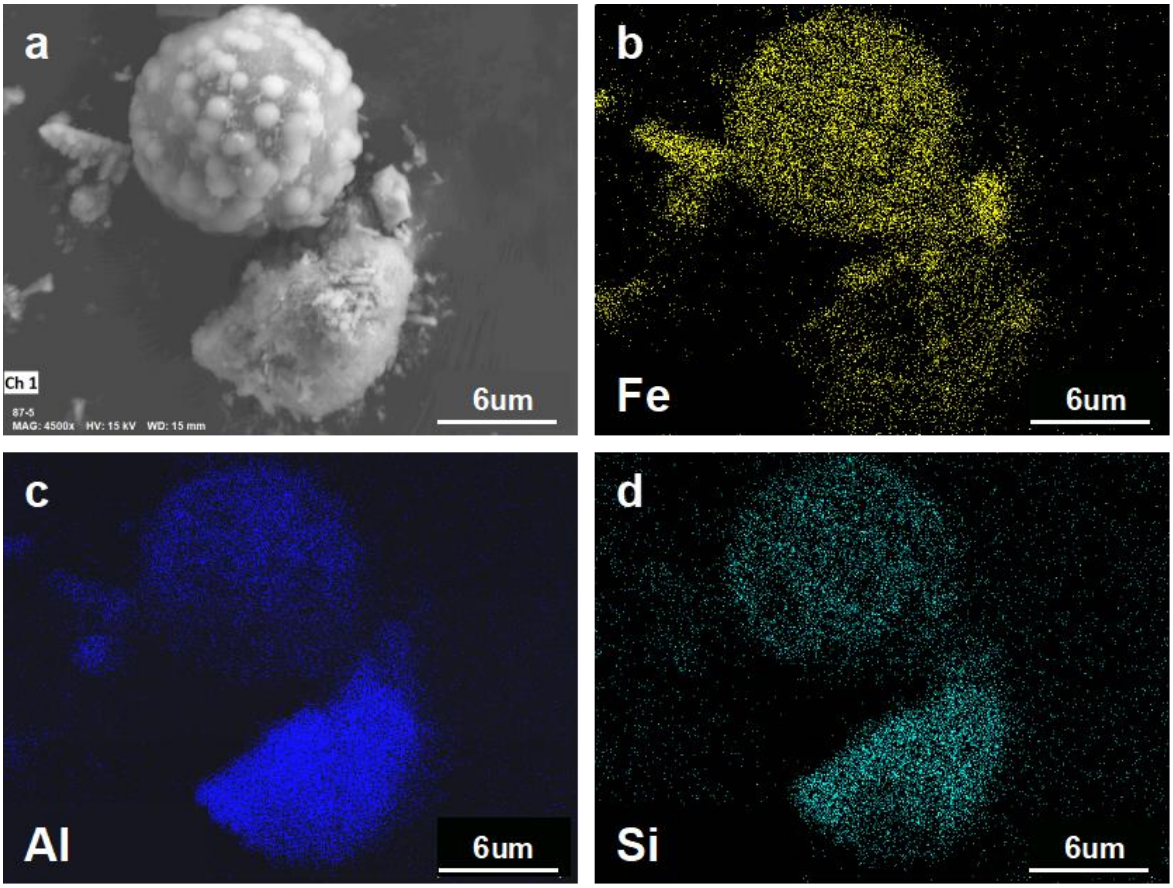

Figure S9. Typical magnetic agglomerates from PCB. The large number of spherical sub-particles on particle surface indicate the continuous agglomeration during combustion process.

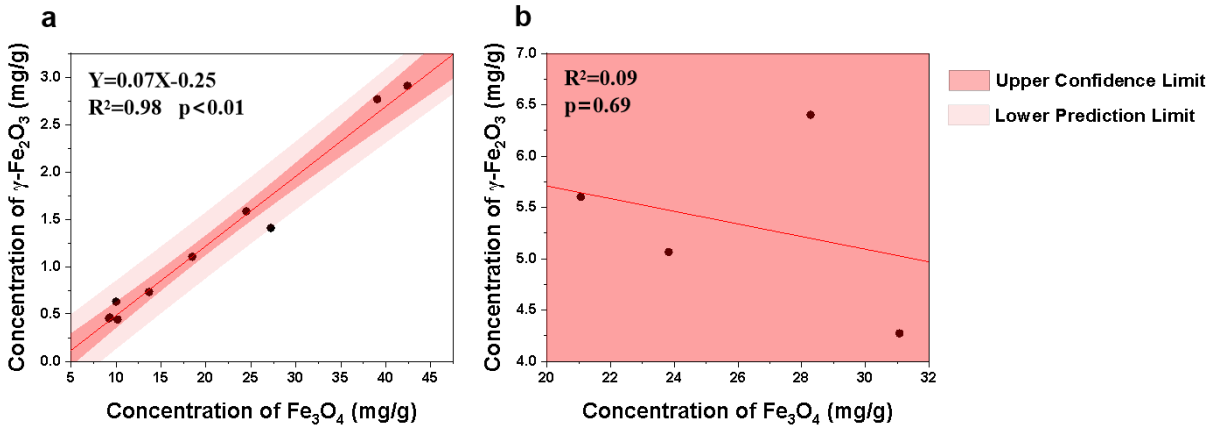

Figure S10. Correlation between the iron concentration of Fe_3O_4 and γ-Fe_2O_3 in FA samples. (a) FA samples collected from PP1 with PCB. (b) FA samples collected from PP2 with FBC.

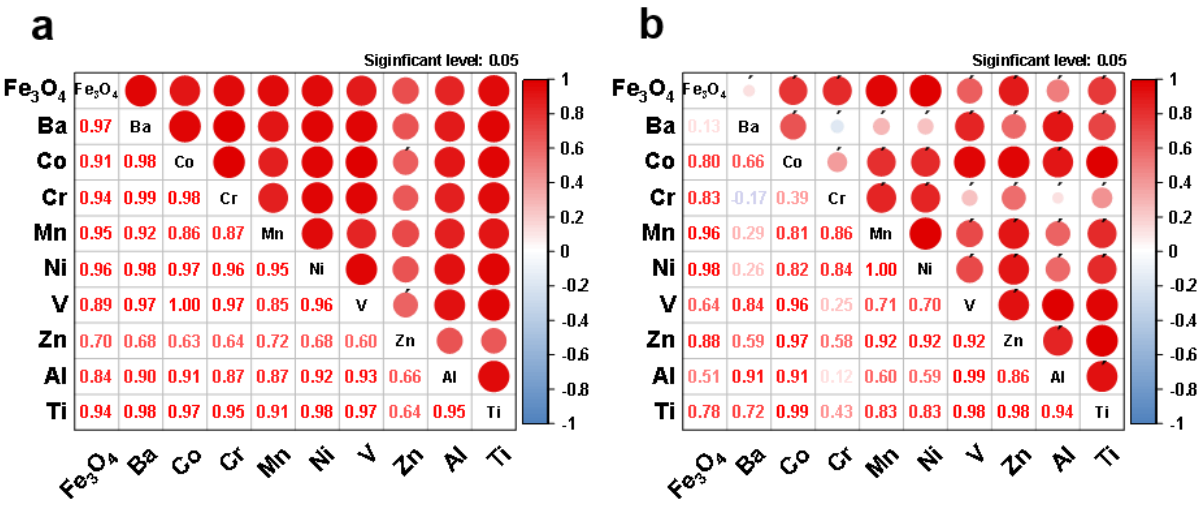

Figure S11. Correlation of the concentration of Fe_3O_4 with its associated elements from (a) PP1 with PCB and (b) PP2 with FBC. The correlations observed in PP1 with pulverized coal boilers were more significant than in PP2 with fluidized bed combustor. The correlation coefficient is given in the left bottom of the chart. The insignificant correlation is marked with apostrophe.